Impact of oxygen on gallium doped germanium

Kuganathan, K., Bracht, H., Davazoglou, K., Kipke, F. & Chroneos, A.

N. Kuganathan, H. Bracht, K. Davazoglou, F. Kipke, and A. Chroneos

ARTICLES YOU MAY BE INTERESTED IN

Mechanisms of boron diffusion in silicon and germanium
Journal of Applied Physics **113**, 031101 (2013); https://doi.org/10.1063/1.4763353

Intrinsic and extrinsic diffusion of phosphorus, arsenic, and antimony in germanium
Journal of Applied Physics **103**, 033508 (2008); https://doi.org/10.1063/1.2837103

Defect and dopant properties in CaMnO₃
AIP Advances **11**, 055106 (2021); https://doi.org/10.1063/5.0048401

AIP Advances

SPECIAL TOPIC: Advances in Low Dimensional and 2D Materials

Call For Papers!

Impact of oxygen on gallium doped germanium

View Online   Export Citation   CrossMark

N. Kuganathan,[1,2,a] H. Bracht,[3] K. Davazoglou,[4] F. Kipke,[3] and A. Chroneos[1,2,b]

AFFILIATIONS

[1] Faculty of Engineering, Environment and Computing, Coventry University, Priory Street, Coventry CV1 5FB, United Kingdom
[2] Department of Materials, Imperial College, London SW7 2AZ, United Kingdom
[3] Institute of Materials Physics, University of Münster, Wilhelm-Klemm-Strasse 10, D-48149 Münster, Germany
[4] Department of Informatics and Telecommunications, National and Kapodistrian University of Athens, GR 15784 Athens, Greece

[a] Author to whom correspondence should be addressed: n.kuganathan@imperial.ac.uk
[b] Electronic mail: ab8104@coventry.ac.uk

ABSTRACT

Germanium (Ge) has advantageous materials properties and is considered as a mainstream material for nanoelectronic applications. Understanding dopant–defect interactions is important to form well-defined doped regions for devices. Gallium (Ga) is a key p-type dopant in Ge. In the present density functional theory study, we concentrate on the structures and electronic structures of Ga doped Ge in the presence of Ge vacancies and oxygen. We provide information on the defect structures and charge transfer between the doped Ga atom and the nearest neighbor Ge atom. The calculations show that the presence of Ga on the Ge site facilitates the formation of nearest neighbor Ge vacancies at 0.75 eV. The formation of interstitial oxygen is endoergic with the formation of −2 charge in both bulk Ge and Ga substituted Ge although the substitution of Ga has slightly less impact on the oxygen interstitial formation.

I. INTRODUCTION

Germanium (Ge) is being considered by the community as it has better carrier mobilities, smaller bandgap, and lower dopant activation temperatures as compared to other technologically relevant group IV semiconductors [i.e., silicon (Si) or silicon germanium ($Si_{1-x}Ge_x$) alloys].[1–3]

Gallium (Ga) is technologically important in Ge as it is a p-type dopant.[1] Ga diffusion in Ge is consistent with the vacancy mechanism as it has a lower diffusion activation enthalpy than Ge self-diffusion.[4–9] Ge is, in many aspects, similar to Si; however, the solubility of oxygen in Czochralski-grown Ge is not as high as in Si.[10,11] At any rate, high oxygen concentrations can be introduced into Ge when there is oxygen gas or H_2O vapor in the growth atmosphere.[1] In Ge, oxygen interstitials (O_i) are electrically inactive; therefore, oxygen is deemed not to be a problematic impurity.[1] At any rate, O_i can interact with vacancies, which are the dominant defects in Ge to form vacancy-oxygen defects (known as A-centers)

although these defects and their properties are not as well understood as in Si.[12–19] The interaction of isovalent atoms with oxygen and vacancies has been investigated in Ge using density functional theory (DFT).[17] In this study, it was shown that O_i bind with nearest neighbor carbon or Si dopants.[17] Interestingly, in a recent study, Kipke *et al.*[20] determined that boron (B) diffusion in Ge is enhanced if the oxygen concentration is high, $>10^{19}$ cm^{-3} (the interesting fact that the heterodiffusion coefficient in a material is enhanced upon adding an increasing concentration of aliovalent dopants has also been observed in previous studies[21–23]). It is therefore anticipated that oxygen will also interact with other p-type dopants, such as Ga.

In this study, structures and electronic structures of Ga doped Ge in the presence of Ge vacancies and oxygen interstitials are discussed with the aid of DFT simulations. The current simulation technique provides information on the defect structures and charge transfer between the doped Ga atom and the nearest neighbor Ge atoms, assisting the interpretation of experimental data.

II. METHODOLOGY

All calculations were performed using a DFT code VASP (Vienna *Ab Initio* Simulation Package).[24] This code solves standard Kohn–Sham equations using plane wave basis sets and projected augmented wave (PAW) pseudopotentials.[25] In all calculations, a plane wave basis set with a cutoff of 500 eV and an 8 × 8 × 8 Monkhorst–Pack[26] k-point mesh were used. The exchange–correlation energy was modeled using the generalized gradient approximation (GGA) scheme as defined by Perdew–Burke–Ernzerhof (PBE).[27] All defect calculations were performed using a 2 × 2 × 2 supercell containing 64 atoms. The conjugate gradient algorithm[28] was used to perform full geometry optimization (both atom positions and lattice constants were relaxed simultaneously). In all relaxed configurations, forces on the atoms were less than 0.001 eV/Å. In order to describe the behavior of the localized Ge *p* states, we included the orbital dependent Coulomb potential (Hubbard U) and the exchange parameter J within the DFT+U calculations, as formulated by Dudarev *et al.*[29] We applied the values of U = 0 eV and J = 3.33 eV to the localized p states of Ge as reported in a previous study.[30]

III. RESULTS AND DISCUSSION

A. Structure of germanium

First, the crystal structure of cubic Ge (space group Fd$\bar{3}$m, No: 227)[31] was relaxed under constant pressure to obtain equilibrium lattice constants to validate the quality of the basis sets and pseudopotentials. In order to obtain a good electronic structure, we used the Hubbard U parameter for *p*-states of Ge. Figure 1 shows the relaxed configuration of bulk Ge and its densities of state plots calculated using GGA and GGA+U methods. Table I reports the calculated lattice parameters and bandgaps together with experimental values.[31,32] There is good agreement between the calculated and experimental values of lattice parameters and bandgap values using the GGA+U approach. As there is a significant deviation between the calculated values using the GGA approach and experimental values, we opted to use the GGA+U method in the defect calculations.

TABLE I. Calculated lattice parameters and bandgaps using GGA and GGA+U methods. The corresponding experimental values are also provided.

Parameters	Calculated			$|\Delta|$ (%)	
	GGA	GGA+U	Expt.	GGA	GGA+U
a = b = c (Å)	5.79	5.60	5.66[31]	2.30	1.06
$\alpha = \beta = \gamma$ (°)	90.0	90.0	90.0[31]	0.00	0.00
V (Å^3)	193.7	175.5	181.0[31]	7.02	3.04
E_{gap} (eV)	0.20	0.70	0.74[32]	72.9	5.40

B. Ga-substituted germanium

A single Ga atom was substitutionally doped on the Ge site. The relaxed structure shows that the Ga atom perfectly forms a tetragonal unit (GaGe$_4$) with almost identical bond lengths and angles to those calculated for the GeGe$_4$ unit in the Ge bulk [see Fig. 2(b)]. This is further confirmed by the charge density plot associated with the doped configuration [see Fig. 2(c)]. The Bader charge analysis[33] shows that Ga loses its outermost three electrons and donates to the nearest neighbor Ge atoms [see Fig. 2(b)]. This is due to the lower ionization potential of Ga (5.9993) than that of Ge (7.8994).[34] Three electrons that are lost by Ga are almost equally distributed. The substitution of Ga leaves three electrons on the Ga atoms [see Fig. 2(d)]. The formation of three electrons in the lattice makes this substituted configuration metallic [see Fig. 2(e)]. The atomic DOS plot of Ga is shown in Fig. 2(f). The states associated with Ga appear in the valence band, inferring the strong bonding nature of Ga with Ge.

The substitution energy for a single Ga atom to replace a single Ge atom was calculated using the following equation:

$$E_{Sub} = E_{(Ga:Ge\_bulk)} + E_{(Ge)} - E_{(Ge\_bulk)} - E_{(Ga)}, \quad (1)$$

where $E_{(Ga:Ge\_bulk)}$ is the total energy of a single Ga atom doped Ge bulk, $E_{(Ge\_bulk)}$ is the total energy of bulk Ge, and $E_{(Ge)}$ and $E_{(Ga)}$ are the energies of Ge and Ga with respect to their bulk structures, respectively. The substitution energy is endothermic (1.72 eV), inferring the strong Ge–Ge bonds.
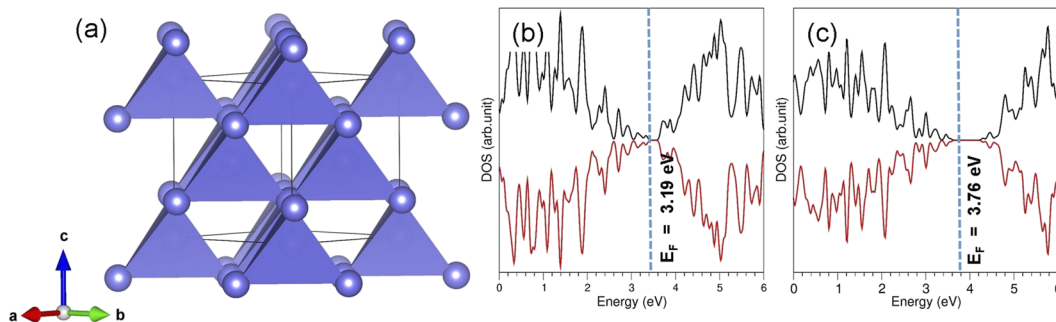

FIG. 1. (a) Relaxed structure of the Ge bulk and (b) and (c) DOS plots calculated using GGA and GGA+U, respectively. Vertical blue dotted lines correspond to the Fermi energy level.
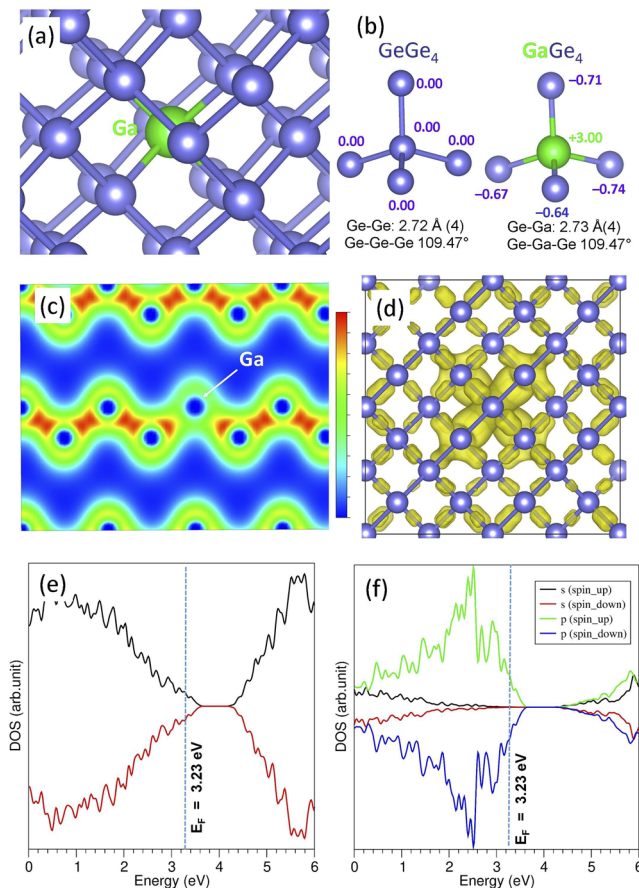
FIG. 2. (a) Relaxed structure of Ga-substituted Ge; (b) tetrahedral units showing bond distances, bond angles, and the Bader charges in the relaxed configurations of Ge and Ga-substituted Ge; (c) charge density plot showing the bonding interaction of Ga; (d) band-decomposed charge density plot associated with Ga; (e) total DOS plot; and (f) atomic DOS plot of Ga.

C. Ga-substituted germanium in the presence of vacancies

The interaction of vacancies with p-type and n-type dopants is an important issue in Ge when considering nanoelectronic applications.[35–42] Here, we considered the doping of Ga in the presence of three different Ge vacancies [first nearest neighbor (FNN), second nearest neighbor (SNN), and third nearest neighbor (TNN)]. The relaxed structures are shown in Fig. 3.

The presence of Ge vacancies significantly changes the Ge–Ga bond distances compared to those calculated in the absence of Ge vacancies [see Figs. 3(d)–3(f)]. A significant reduction in the Ge–Ga bond distances (by ~0.30 Å) is observed. In the first configuration (FNN), Ga forms a distorted trigonal planar (or trigonal pyramid) structure with the bond angle of 112.48° and the bond length of 2.43 Å. The Bader analysis shows that three electrons lost by Ga are distributed almost equally to the nearest neighbor Ge atoms. In the case of the second configuration [see Fig. 3(b)], a tetrahedral unit is

formed by Ga. This is because of the Ge vacancy located slightly away from Ga. There is a slight perturbation in the bond lengths and bond angles [see Fig. 3(e)]. The positive Bader charge (+3.00) is observed for Ga as expected, and three electrons are shared by the four nearest neighbor Ge atoms. In the TNN configuration [see Fig. 3(c)], four equivalent Ge–Ga bond distances are noted. The bond angles range between 107° and 110°. The formation of +3 charge is observed on Ga, and the lost electrons are gained by the adjacent Ge atoms [see Fig. 3(f)]. The charge density plots show the strong bonding nature of Ge together with the positions of the Ga and Ge vacancies.

The substitution energy of Ga in the presence of Ge vacancies and binding energy to form the FNN configuration from other two configurations are calculated (see Table II). Calculations reveal that the FNN configuration is energetically more stable than the SNN configuration (at 0.64 eV) and the TNN configuration (at 0.75 eV). The energy difference between the SNN and TNN configurations is 0.14 eV, indicating the stability of the SNN configuration over the TNN configuration. The substitution becomes easier (at 0.75 eV) in the presence of FNN Ge vacancies than in the absence of Ge vacancies. Once the position of vacancy is slightly shifted, the substitution energy increases. In the case of the TNN, the substitution energy is identical to the substitution energy calculated in the absence of Ge vacancies. This indicates that the substitution was not affected by the TNN Ge vacancy.

Figure 4 shows the total DOS, atomic DOS plots, and band-decomposed charge density plots. The Fermi energy calculated for the FNN configuration is unaffected compared to that calculated for the Ga doped Ge bulk configuration [see Fig. 4(a)]. In the other two configurations, a slight reduction in the Fermi energy is noted. In all three cases, the final configurations exhibit metallic character. This is due to the electron charge density localized on the Ge atoms closer to Ga. The atomic DOS plots calculated for Ga show that both s and p states are strongly localized in the valence band.

D. Oxygen interstitial in the Ge bulk and its impact on the substitution of Ga

In this section, we discuss the incorporation of a single oxygen atom as an interstitial atom in the pristine Ge bulk and Ga-substituted Ge bulk. In the latter case, we considered two different configurations. In the first configuration (O_i:Ga_NN), the oxygen atom interacts with nearest neighbor Ga [see Fig. 5(b)]. In the second configuration (O_i:Ga_NNN), the doped Ga is present as the next nearest neighbor to the oxygen interstitial. The relaxed structures are shown in Fig. 5.

There is a strong bond nature between the interstitial oxygen and the adjacent Ge atoms [see Fig. 5(a)]. This is evidenced by the shorter bond lengths (1.79 Å) and significant charge transfer between the oxygen and Ge atoms [see Fig. 5(d)]. The interstitial oxygen is two-coordinated, forming a bent (or V-shape) structure with a Ge–O–Ge bond angle of 137.3°. The Bader charge on the oxygen atom is −1.92, inferring the formation of the O^{2-} ion. The gain of two electrons is mainly from the two adjacent Ge atoms attached to the oxygen atom [see Fig. 5(d)]. In the first
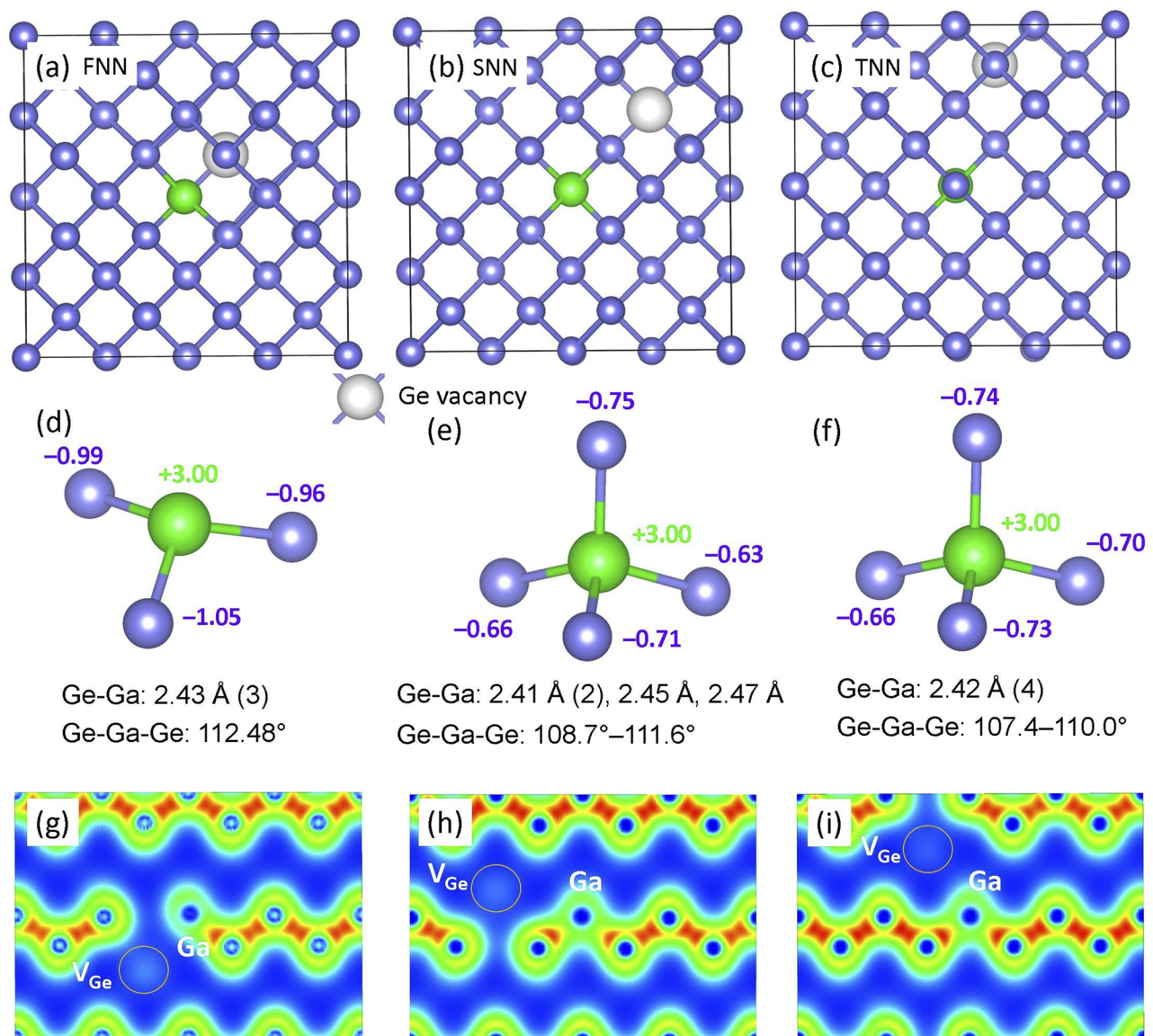
FIG. 3. (a)–(c) Three different configurations of Ga substituted bulk Ge in the presence of a Ge vacancy; (d)–(f) their bond distances, bond angles, and Bader charges; and (g)–(i) corresponding charge density plots associated with the Ga–V_{Ge} pair.

TABLE II. Substitution energy of Ga in the presence of Ge vacancy, relative energy of each configuration with respect to the FNN configuration, and binding energy for the formation of a stable configuration from the other configuration.

	Configuration		
	FNN	SNN	TNN
Substitution energy (eV)	1.03	1.64	1.78
Relative energy (eV)	0.00	0.61	0.75
	SNN → FNN	TNN → FNN	TNN → SNN
Binding energy (eV)	−0.64	−0.75	−0.14

configuration of an oxygen interstitial interacting nearest neighbor Ga (O_i:Ga_NN), the oxygen atom is strongly bonded to the nearest Ge and Ga [see Fig. 5(b)]. The negative charge (−1.85) on the oxygen atom is donated by Ge and Ga atoms attached to it according to the Bader charges [see Fig. 5(e)]. The Ga–O and Ge–O bond distances are calculated to be 1.87 and 1.77 Å, respectively, indicating the different ionization potentials. The Ge–O–Ga bond angle is slightly contracted. In the second configuration (O_i:Ga_NNN), the geometry of the Ge–O–Ge unit is almost the same as noted in the configuration where oxygen is incorporated into the bulk Ge. The Bader charge on the oxygen atom confirms the formation of −2 charge.
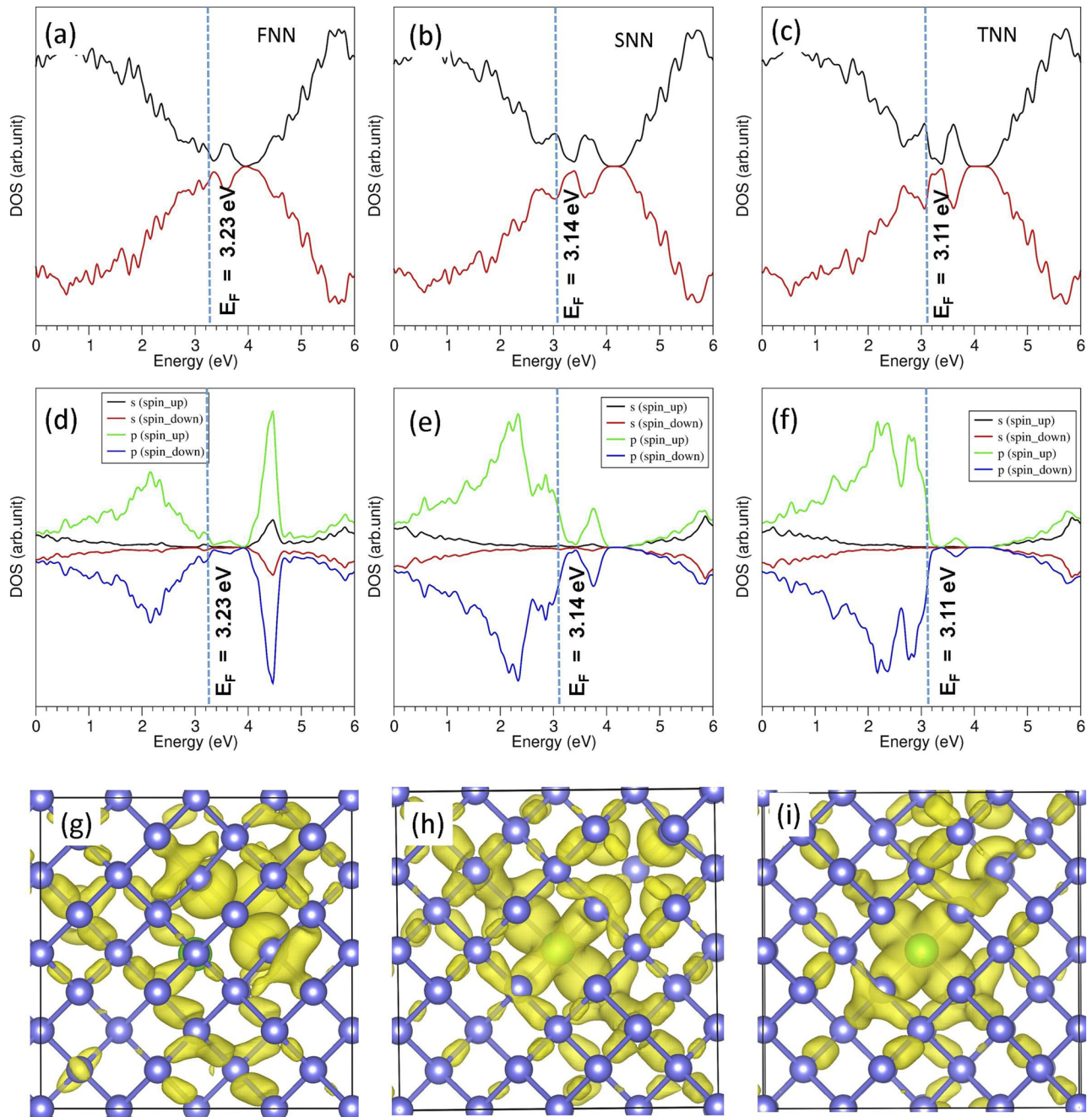
FIG. 4. (a)–(c) Total densities of states calculated for three different Ga–V$_{Ge}$ pairs as shown in Fig. 3, (d)–(f) corresponding atomic DOS plots calculated for each configuration, and (g)–(i) corresponding band-decomposed charge density plots around the Ga atoms.

The incorporation energy of the oxygen atom into the bulk Ge was calculated using the following equation:

$$E_{inc} = E_{O@Ge\_bulk} - E_{Ge\_bulk} - E_{\frac{1}{2}O_2}, \tag{2}$$

where $E_{O@Ge\_bulk}$ is the total energy of an oxygen atom incorporated into the bulk Ge, E_{Ge_bulk} is the total energy of the bulk Ge, and $E_{\frac{1}{2}O_2}$ is the total energy of half-molecule of oxygen. The incorporation energy is exothermic in all cases, meaning that oxygen is more stable inside the Ge bulk than its isolated molecular form
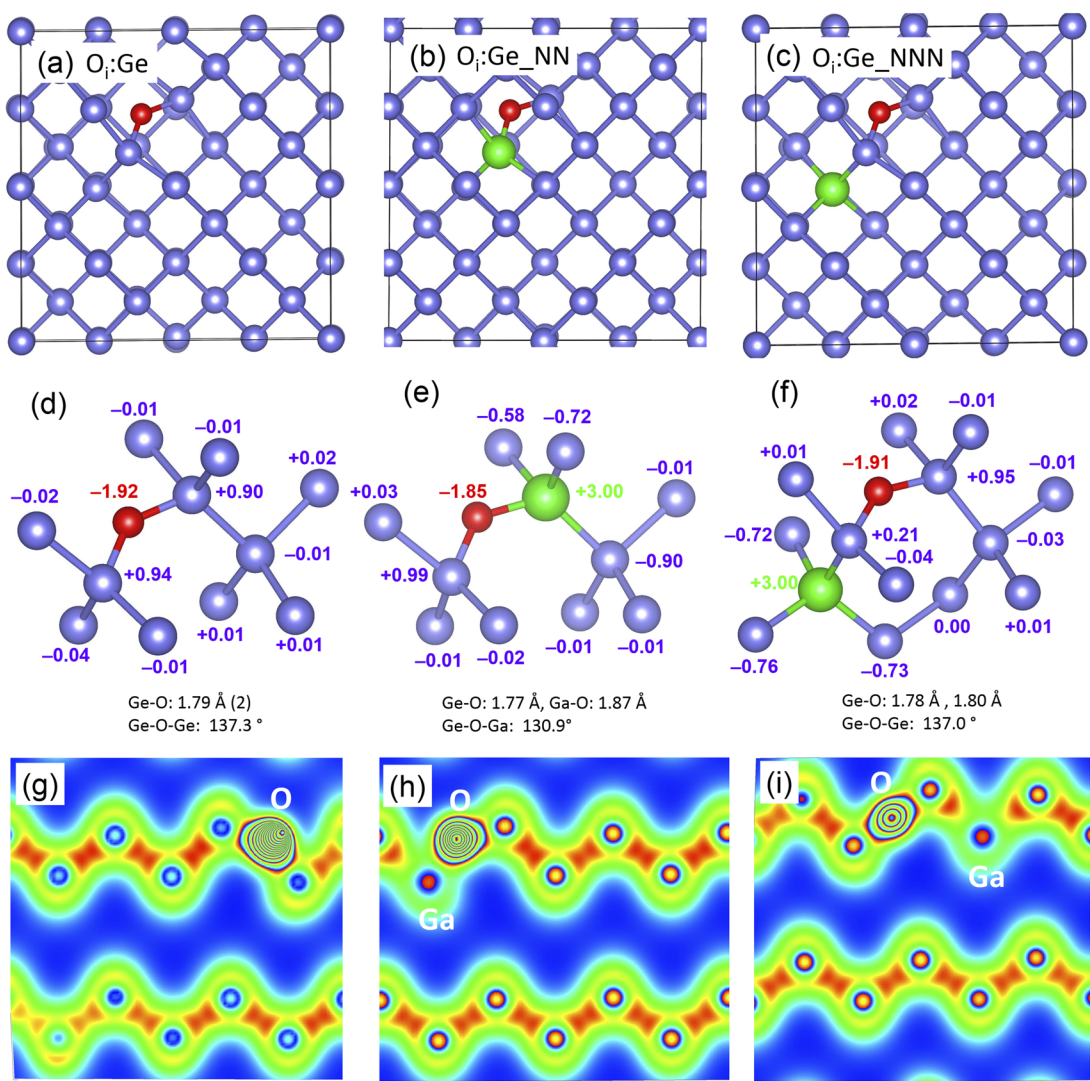
FIG. 5. Relaxed configurations of an oxygen interstitial in (a) bulk Ge, (b) nearest neighbor Ga substituted in bulk Ge, and (c) next nearest neighbor Ga substituted in bulk Ge; (d)–(f) corresponding bond lengths, bond angles, and the Bader charges on the selected atoms in the relaxed configurations; and (g)–(i) charge density plots showing the interaction of the oxygen interstitial with Ge and Ga.

(see Table III). The binding energy to form the O_i:Ga_NN configuration from O_i:Ga_NNN is −0.03 eV.

Figure 6 shows the total and atomic DOS plots and band-decomposed charge density plots around the O atoms. The total DOS calculated for the oxygen interstitial in the Ge bulk shows that the oxygen incorporated configuration is a semi-conductor with a bandgap of 0.70 eV. However, Ga-doped configurations exhibit metallic character due to the electron density formed on the Ge atoms. Atomic DOS plots calculated for the incorporated oxygen atom show that its p-states are localized in the valence band, inferring the strong bonding between Ge and O. This is further confirmed by the band-decomposed charge density plots around the O atoms.

TABLE III. Incorporation energies of the oxygen atom in the bulk Ge and Ga substituted Ge bulk, relative energies, and the binding energy to form O_i:Ga_NN from O_i:Ga_NNN.

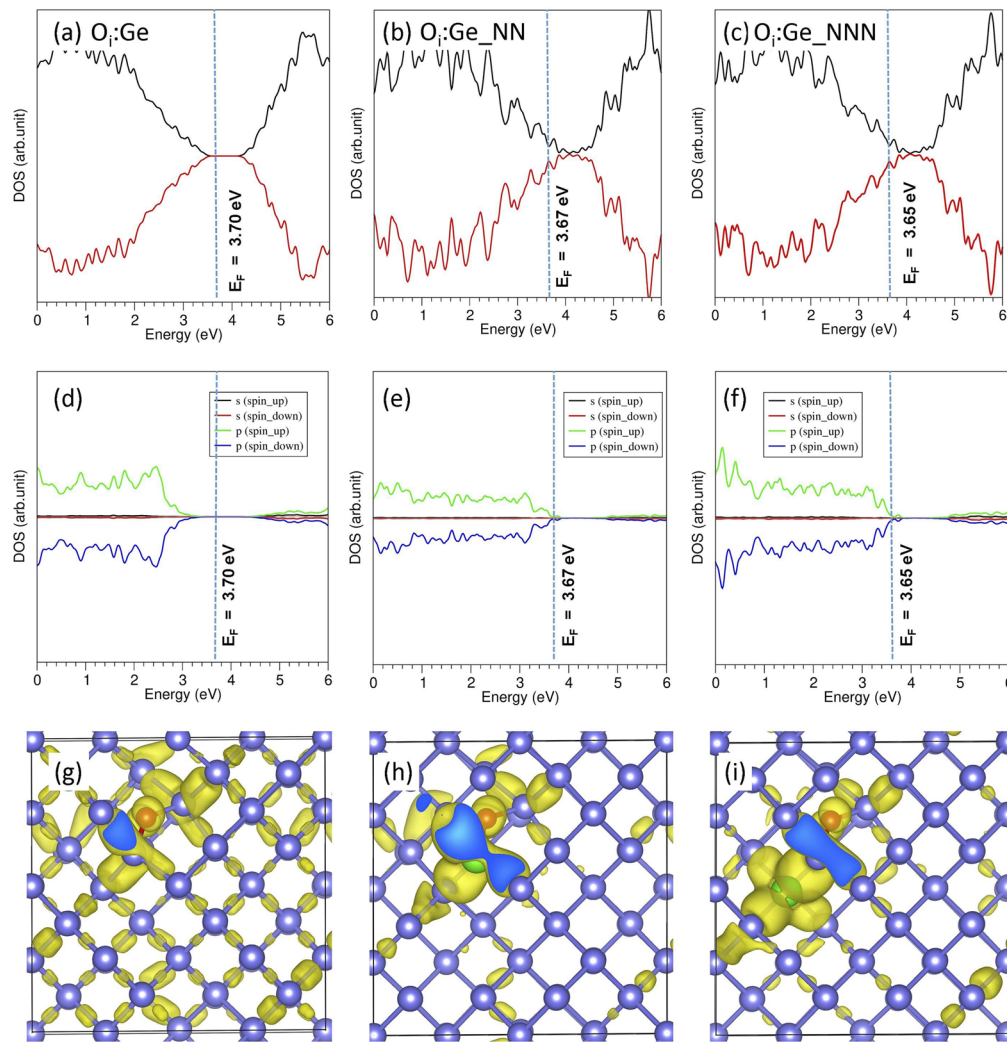|	Configurations		
	O_i:Ge	O_i:Ga_NN	O_i:Ga_NNN
Incorporation energy (eV)	−1.24	−1.14	−1.11
Relative energy (eV)	⋯	0.00	0.03
	O_i:Ga_NNN → O_i:Ga_NN		
Binding energy (eV)	−0.03		

FIG. 6. Total densities of states calculated for an oxygen interstitial in (a) bulk Ge, (b) nearest neighbor Ga substituted in bulk Ge, and (c) next nearest neighbor Ga substituted in bulk Ge; (d)–(f) corresponding atomic DOS plots calculated for each configurations; and (g)–(i) corresponding band-decomposed charge density plots around the O atoms.

IV. CONCLUSIONS

In the present study, we employed advanced DFT modeling to predict the interaction of Ga with vacancies and O_i. It was shown that the substitution of Ga promotes the formation of nearest neighbor Ge vacancies at 0.75 eV. Exoergic incorporation energies are calculated for the interstitial oxygen in the pristine Ge and Ga substituted Ge. Such favorable incorporation is further confirmed by the negative Bader charge of −2 on the incorporated oxygen. The oxygen interstitial formation has less impact on the Ga doping on Ge. The semiconducting nature of Ge vacancy or O_i in the Ge bulk is converted into metallic upon Ga substitution.

ACKNOWLEDGMENTS

The authors declare that there is no competing financial interest.

DATA AVAILABILITY

The data that support the findings of this study are available from the corresponding author upon reasonable request.

REFERENCES

[1] C. Claeys and E. Simoen, *Germanium-based Technologies: From Materials to Devices* (Elsevier, 2007).

[2] W.-S. Jung, J.-H. Park, A. Nainani, D. Nam, and K. C. Saraswat, Appl. Phys. Lett. **101**, 072104 (2012).

[3] A. Chroneos and H. Bracht, Appl. Phys. Rev. **1**, 011301 (2014).

[4] P. Dorner, W. Gust, A. Lodding, H. Odelius, and B. Predel, Acta Metall. **30**, 941 (1982).

[5]P. Dorner, W. Gust, A. Lodding, H. Odelius, B. Predel, and U. Roll, Z. Metallkd. **73**, 325 (1982).

[6]U. Södervall, H. Odelius, A. Lodding, U. Roll, B. Predel, W. Gust, and P. Dorners, Philos. Mag. A **54**, 539 (1986).

[7]I. Riihimäki, A. Virtanen, S. Rinta-Anttila, P. Pusa, J. Räisänen, and The ISOLDE Collaboration, Appl. Phys. Lett. **91**, 091922 (2007).

[8]E. Hüger, U. Tietze, D. Lott, H. Bracht, D. Bougeard, E. E. Haller, and H. Schmidt, Appl. Phys. Lett. **93**, 162104 (2008).

[9]R. Kube, H. Bracht, A. Chroneos, M. Posselt, and B. Schmidt, J. Appl. Phys. **106**, 063534 (2009).

[10]A. Chroneos, H. Bracht, R. W. Grimes, and B. P. Uberuaga, Appl. Phys. Lett. **92**, 172103 (2008).

[11]W. Kaiser and C. D. Thurmond, J. Appl. Phys. **32**, 115 (1961).

[12]J. A. Baldwin, Jr., J. Appl. Phys. **36**, 793 (1965).

[13]G. D. Watkins and J. W. Corbett, Phys. Rev. **121**, 1001 (1961).

[14]V. P. Markevich, I. D. Hawkins, A. R. Peaker, V. V. Litvinov, L. I. Murin, L. Dobaczewski, and J. L. Lindström, Appl. Phys. Lett. **81**, 1821 (2002).

[15]V. P. Markevich, V. V. Litvinov, L. Dobaczewski, J. L. Lindström, L. I. Murin, S. V. Vetrov, I. D. Hawkins, and A. R. Peaker, Physica B **340–342**, 844 (2003).

[16]A. Chroneos and C. A. Londos, J. Appl. Phys. **107**, 093518 (2010).

[17]A. Chroneos, C. A. Londos, and H. Bracht, Mater. Sci. Eng. B **176**, 453 (2011).

[18]H. Wang, A. Chroneos, C. A. Londos, E. N. Sgourou, and U. Schwingenschlögl, Sci. Rep. **4**, 4909 (2014).

[19]A. Chroneos, E. N. Sgourou, C. A. Londos, and U. Schwingenschlögl, Appl. Phys. Rev. **2**, 021306 (2015).

[20]F. Kipke, T. Südkamp, J. K. Prüßing, D. Bougeard, and H. Bracht, J. Appl. Phys. **127**, 025703 (2020).

[21]P. A. Varotsos and K. D. Alexopoulos, *Thermodynamics of Point Defects and their Relation with Bulk Properties* (North Holland, Amsterdam, 1986).

[22]K. Alexopoulos and P. Varotsos, Phys. Rev. B **24**, 3606–3609 (1981).

[23]A. Chroneos, C. A. Londos, E. N. Sgourou, and P. Pochet, Appl. Phys. Lett. **99**, 241901 (2011).

[24]G. Kresse and D. Joubert, Phys. Rev. B **59**, 1758–1775 (1999).

[25]P. E. Blöchl, Phys. Rev. B **50**, 17953–17979 (1994).

[26]H. J. Monkhorst and J. D. Pack, Phys. Rev. B **13**, 5188–5192 (1976).

[27]J. P. Perdew, K. Burke, and M. Ernzerhof, Phys. Rev. Lett. **77**, 3865–3868 (1996).

[28]W. H. Press, S. A. Teukolsky, W. T. Vetterling, and B. P. Flannery, *Numerical Recipes in C: The Art of Scientific Computing*, 2nd ed. (Cambridge University Press, 1992).

[29]S. L. Dudarev, G. A. Botton, S. Y. Savrasov, C. J. Humphreys, and A. P. Sutton, Phys. Rev. B **57**, 1505 (1998).

[30]H. Tahini, A. Chroneos, R. W. Grimes, U. Schwingenschlögl, and H. Bracht, Appl. Phys. Lett. **99**, 072112 (2011).

[31]A. Smakula and J. Kalnajs, Phys. Rev. **99**, 1737–1743 (1955).

[32]S. M. Sze, *The Physics of Semiconductor Devices* (Wiley, New York, 2006).

[33]R. F. W. Bader, Theor. Chem. Acc. **105**, 276–283 (2001).

[34]*CRC Handbook of Chemistry and Physics*, 86th ed., edited by D. R. Lide (National Institute of Standards and Technology; CRC Press; Taylor and Francis Group, Boca Raton, FL, 2005), p. 2544.

[35]S. Uppal, A. F. W. Willoughby, J. M. Bonar, N. E. B. Cowern, T. Grasby, R. J. H. Morris, and M. G. Dowsett, J. Appl. Phys. **96**, 1376 (2004).

[36]A. Chroneos, D. Skarlatos, C. Tsamis, A. Christofi, D. S. McPhail, and R. Hung, Mater. Sci. Semicond. Process. **9**, 640–643 (2006).

[37]A. Chroneos, Phys. Status Solidi B **244**, 3206–3210 (2007).

[38]A. Chroneos, H. Bracht, R. W. Grimes, and B. P. Uberuaga, Mater. Sci. Eng. B **154–155**, 72–75 (2008).

[39]E. Simoen and J. Vanhellemont, J. Appl. Phys. **106**, 103516 (2009).

[40]A. Chroneos, R. W. Grimes, and H. Bracht, J. Appl. Phys. **106**, 063707 (2009).

[41]G. Impellizzeri, S. Mirabella, A. Irrera, M. G. Grimaldi, and E. Napolitani, J. Appl. Phys. **106**, 013518 (2009).

[42]G. Impellizzeri, S. Boninelli, F. Priolo, E. Napolitani, C. Spinella, A. Chroneos, and H. Bracht, J. Appl. Phys. **109**, 113527 (2011).